Modelling and Analysis of Power Imbalance Impact on Digital Subcarrier Multiplexed Coherent PON

(Article begins on next page)

Modelling and Analysis of Power Imbalance Impact on Digital Subcarrier Multiplexed Coherent PON

1st Safana Alzoubi
Department of Electronics and Telecommunications
Politecnico di Torino
Torino, Italy

2nd Roberto Gaudino
Department of Electronics and Telecommunications
Politecnico di Torino
Torino, Italy

***Abstract*—Coherent transmission is strongly considered for very-high speed PON (the next PON generation as defined by ITU-T) to meet the ever-increasing bandwidth demands (at least 200 Gbps), benefiting from higher modulation formats and improved DSP-based receiver sensitivity. Digital subcarrier multiplexing (DSCM), as a variant of coherent PON, can further provide enhanced flexibility and lower latency, making it a promising solution for 5G/6G fronthaul applications. However, existing point-to-point DSCM systems must be adapted to PON-specific challenges, particularly the large power dynamic range inherent to point-to-multipoint shared infrastructure. In this paper, we investigate the impact of upstream subcarrier power imbalance (PI) in DSCM-PON systems considering two physical impairments: transmitter pulse-shaping filter and subcarrier frequency offset. We adapt and employ the frequency-resolved semi-analytical model to quantify the DSCM PON performance degradation due to PI and further validate it against time-domain numerical simulations. The proposed model shows high accuracy, with a discrepancy below 0.5 dB compared to numerical results. Our findings highlight that PI can become a critical limitation in DSCM-PON performance and should be carefully considered in system dimensioning and physical-layer design.**

***Index Terms*—Coherent passive optical network (PON), digital sub-carrier multiplexing (DSCM), power imbalance.**

I. Introduction

Future passive optical networks are anticipated to deliver data rates beyond 200 Gbps per wavelength, while accommodating high optical distribution losses and greater flexibility, without compromising the cost-effectiveness of current PON solutions. To address these requirements, a working group within the International Telecommunication Union (ITU-T) is currently leading the Very High Speed PON (VHSP) initiative, which evaluates the technical options for next-generation PON systems [1]. Within this framework, coherent transmission and its digital subcarrier multiplexing (DSCM) variant are being considered as promising candidates for future PON deployments [2], [3]. DSCM-PON exploits amplitude, phase, and polarization to improve flexibility while enabling the use of lower-bandwidth optical network units (ONUs) [4]. Compared to single-carrier coherent PON, DSCM-based coherent PON can provide lower latency and increased flexibility. While DSCM has been widely investigated in point-to-point systems, deploying it in point-to-multipoint PONs remains challenging due to additional system constraints [5], including the upstream burst-mode design, laser control in ONUs, and the large power dynamic range in PON systems, which can reach up to 20 dB in the optical line terminal (OLT) upstream receiver (RX). Conventionally, power dynamics in burst time division multiplexing (TDM)-PON are controlled via automatic gain control (AGC) in the trans-impedance amplifier (TIA); however, this is more difficult in DSCM because, in addition to burst TDM, the subcarriers (SCs) are mixed in the time domain, and thus proper consideration and pre-leveling of the ONU transmitted power is required [6]. On the other hand, since each ONU employs its own laser, frequency control mechanisms are essential to avoid inter-subcarrier interference while maintaining spectral efficiency, especially given the random laser frequency drifts ranging from MHz up to GHz [7], [8].

Given these challenges in DSCM PON systems, we investigate in this paper the impact of upstream power imbalance (PI) on inter-subcarrier interference arising from two relevant physical impairments: (i) transmitter (TX) pulse-shaping filter parameters, namely the roll-off factor and filter length, and (ii) TX laser frequency offset (FO). A short pulse-shaping filter results in fewer taps and, consequently, fewer multiplications, leading to reduced complexity and energy consumption, but at the expense of increased ripples in the frequency response, particularly for low roll-off factors. Conversely, a longer filter provides a more accurate impulse response at the cost of a higher number of multiplications and increased complexity. Increasing the roll-off factor, on the other hand, leads to a larger occupied bandwidth per SC and, consequently, an increased overall signal bandwidth. In addition, TX laser FO, although it can be compensated in the receiver DSP through coarse and fine FO estimation for the shifted subcarrier, it does not eliminate the interference imposed on other subcarriers. Increasing the guard band between subcarriers can mitigate this interference, but at the cost of a larger overall signal bandwidth and reduced spectral efficiency.

In this work, we consider DSCM upstream transmission with only frequency division multiplexing (FDM), rather than time-frequency division multiplexing (TFDM), to focus on the impact of power imbalance between subcarriers, as detailed in Section II, where we assume dedicated SC groups per ONU. The extension to TFDM, including burst-mode transient effects and time-domain mixing, is left for future work. In Section III, we employ the frequency-resolved semi-analytical model

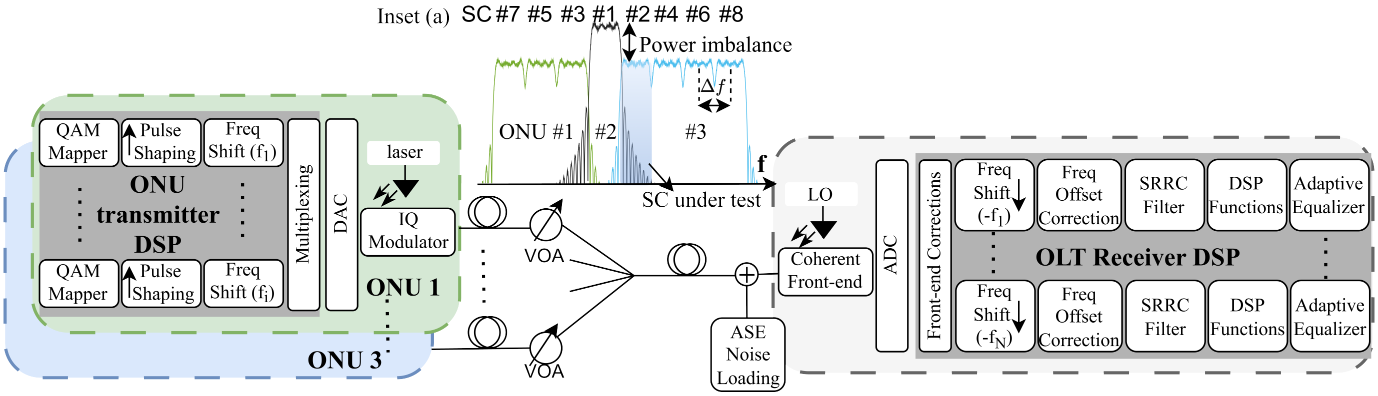

Fig. 1: Block diagram of the upstream signal processing in a DSCM PON with three ONUs. Inset (a) illustrates the OLT received SCs with power imbalance. ONU: optical network unit; DAC: digital-to-analog converter; VOA: variable optical attenuator; ASE: amplified spontaneous emission; LO: local oscillator; ADC: analog-to-digital converter; OLT: optical line terminal. SRRC: square-root raised cosine.

proposed in [9] to evaluate the impact of SC PI in DSCM PON. We then validate the accuracy of the model through numerical simulations in Section IV, and further examine the resulting performance degradation due to the combined effects of linear crosstalk and SC PI. Addressing this PI is essential for DSCM-PON network dimensioning, ONU power pre-leveling, and the appropriate design of SC frequency spacing and physical-layer transmission specifications. Other impairments, such as TX/RX IQ imbalances, quantization noise, laser phase noise, chromatic dispersion, and fiber nonlinearities, are not considered, as they are outside the scope of the present work.

II. Digital Subcarrier multiplexed coherent PON system setup

The ONUs transmitter and the OLT receiver are shown in Fig. 1, representing the upstream direction signal processing in a DSCM coherent PON. For simplicity, we assume a system with $N = 8$ SCs, ordered as shown in the inset of Fig. 1, where the numbers represent the SC indices, and three ONUs, where ONU#1 uses SC#7,5,3, ONU#2 uses SC#1 and ONU#3 uses the remaining SCs. This setup allows us to isolate the impact of a single SC on its neighbor, namely SC# 1 on SC#2. Each ONU generates a set of complex base-band QAM-modulated signals with a symbol rate of R_s, which are Nyquist pulse-shaped using a square-root raised cosine (SRRC) filter with roll-off factor of ρ, and a filter length of L symbols. In each ONU transmitter, the digital signals are then frequency up-shifted to their respective SC center frequencies, where the spacing between adjacent SC center frequencies is defined as $\Delta f = R_s(1 + \rho)$ as shown in the SC inset in Fig. 1. The SCs are subsequently DSP multiplexed and passed through the digital-to-analog converter, followed by the optical IQ modulator. The resulting optical signal from each ONU i may suffer from a transmitter laser FO δ_i, which should be controlled via local or remote feedback mechanisms [8] to mitigate interference between adjacent SCs. Signals from ONUs occupying distinct SCs propagate through different fiber paths, experiencing different lengths and losses, and are then combined via passive power splitters to propagate through the shared fiber. At the input of the OLT receiver, the optical signal is loaded with amplified spontaneous emission (ASE) noise. While it is not a standard practice to use amplifiers in coherent PON, it is sometimes used to increase power budget such as in [6]. The main performance metric used in this paper will thus be the optical signal to noise ratio (OSNR) required to reach a given BER target, and the resulting OSNR penalty due to the physical layer impairments analyzed in this paper. It was demonstrated in [10], [11] that for a non-optically amplified coherent receiver, the same penalty in dB will become a received optical power (ROP) penalty in terms of sensitivity at the same BER target. Consequently, the curves presented in this paper as "OSNR penalty in dB" can also be interpreted as "ROP penalty" in non-optically amplified receivers.

The received optical signal is first coherently detected and passed through an analog-to-digital converter before being processed by the digital signal processor (DSP). The received DSCM signal initially undergoes front-end corrections, after which each SC is frequency down-shifted to base-band, and down-sampled to 2 samples per symbol. Each SC is then processed through the DSP chain for coherent detection, including chromatic dispersion compensation, FO estimation and correction, filtering, carrier phase compensation, and adaptive equalization to recover the individual SCs.

III. Modelling Power Imbalance in DSCM coherent transmission

The block diagram of the DSCM coherent PON considered in the frequency-resolved semi-analytical model is shown in Fig. 2. The proposed model is based on the frequency-resolved coherent transmission model introduced in [12] and its extension to DSCM transmission presented in [9]. The assumptions in [9] are retained, while only considering ASE noise and inter-subcarrier crosstalk originating from the two neighboring SCs. Nevertheless, the model can be extended to include additional impairments such as the optical filtering, RX bandwidth limitation, electrical noise and RX imperfections, as discussed for coherent transmission in [13], where it has demonstrated accuracy and significantly reduced computational time compared to time-domain simulations.

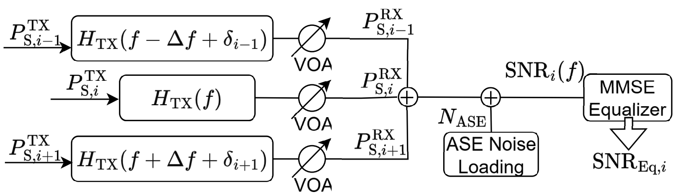

Fig. 2: Block diagram of the considered frequency-resolved model for DSCM coherent PON, with i denoting the SC under test and $i \pm 1$ denoting its neighboring SCs. VOA: variable optical attenuator; ASE: amplified spontaneous emission; SNR: signal to noise ratio; and MMSE: minimum mean square error.

In the proposed model, the SRRC filter is implemented as a finite impulse response (FIR) filter by truncating its infinite impulse response to a duration determined by the filter length in symbols. The corresponding frequency response for the SC under test i, denoted by $H_{\mathrm{TX}}(f)$, is obtained numerically by computing the discrete-time Fourier transform of the truncated impulse response. This pulse-shaping frequency response is then shifted by $\pm\Delta f$ to generate the frequency responses of the neighboring SCs $i \pm 1$, i.e. $H_{\mathrm{TX}}(f \pm \Delta f)$. In addition, TX laser FOs are modeled by further shifting the signal spectra of the neighboring SCs by $\delta_{i\pm1}$, corresponding to the FO of the $(i \pm 1)$-th SC. Consequently, for the two neighboring SCs, the frequency responses become $H_{\mathrm{TX}}\left(f - \Delta f + \delta_{i-1}\right)$ and $H_{\mathrm{TX}}\left(f + \Delta f + \delta_{i+1}\right)$. Figure 3 further illustrates the frequency response of the pulse-shaping filter for the SC under test and its neighboring SCs, showing how the deployed filter length affects the adjacent SCs through frequency ripples. The SC FO is also shown in Fig. 3 as a frequency-profile shift of the left SC.

Here, the transmitted power of the i^{th} SC is denoted by $P^{\mathrm{TX}}_{\mathrm{S},i}$, while the received power is denoted by $P^{\mathrm{RX}}_{\mathrm{S},i}$. The same notation applies to the neighboring SCs $i+1$ and $i-1$. The OLT receives the three SCs combined with ASE noise, denoted by N_{ASE}, which are then processed to obtain the frequency-resolved signal-to-noise ratio $\mathrm{SNR}_i(f)$ and, subsequently, the resulting minimum mean square error (MMSE) equalized SNR $\mathrm{SNR}_{\mathrm{EQ},i}$ for the i^{th} SC.

Under these assumptions, the frequency-resolved signal-to-noise ratio at the input of the receiver can be expressed as

$$\mathrm{SNR}_i(f) = \frac{P^{\mathrm{RX}}_{\mathrm{S},i}\left|H_{\mathrm{TX}}(f)\right|^2}{N_{\mathrm{ASE}} + N_{\mathrm{XT},i}(f)}, \tag{1}$$

where N_{ASE} is evaluated as $P^{\mathrm{RX}}_{\mathrm{S},i}/\mathrm{OSNR}$, with $P^{\mathrm{RX}}_{\mathrm{S},i}$ as previously defined the SC under test received signal power, and OSNR defined over a bandwidth equal to the SC symbol rate R_s. The crosstalk term $N_{\mathrm{XT},i}(f)$ accounts for the two neighboring SCs $i+1$ and $i-1$, including their respective received powers and FOs, and is given by

$$\begin{aligned} N_{\mathrm{XT},i}(f) = {} & P^{\mathrm{RX}}_{\mathrm{S},i-1}\left|H_{\mathrm{TX}}\left(f - \Delta f + \delta_{i-1}\right)\right|^2 \\ & + P^{\mathrm{RX}}_{\mathrm{S},i+1}\left|H_{\mathrm{TX}}\left(f + \Delta f + \delta_{i+1}\right)\right|^2 . \end{aligned} \tag{2}$$

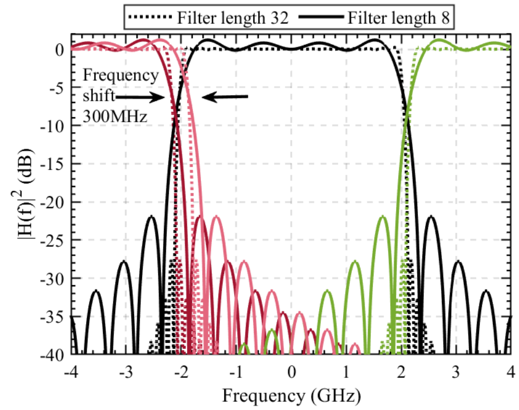

Fig. 3: Transmitter pulse frequency responses for the SC under test and its neighboring SCs in the frequency-resolved model, for a roll-off factor of 0.05 and two filter lengths, with and without a 300 MHz frequency offset in the left SC. The legend applies to all SCs.

The SNR at the output of the adaptive equalizer is then obtained by evaluating the frequency-resolved input SNR as

$$\mathrm{SNR}_{\mathrm{EQ},i} = \frac{1}{T\int_{-\frac{1}{2T}}^{\frac{1}{2T}}\left[1 + \sum_{\mu}\mathrm{SNR}_i\left(f - \frac{\mu}{T}\right)\right]^{-1}\mathrm{d}f} - 1, \tag{3}$$

where T denotes the SC symbol duration and μ represents the integer number of spectral foldings. The resulting $\mathrm{SNR}_{\mathrm{EQ},i}$ is subsequently used to compute the bit-error rate (BER) according to the expressions for the corresponding modulation format, for example, the BER fo 16-QAM is given by $\mathrm{BER}_i = (3/8)\mathrm{erfc}\left(\sqrt{\mathrm{SNR}_{\mathrm{EQ},i}/10}\right)$.

IV. Simulation Results and Discussion

In this section, we compare the semi-analytical model described in Section III with numerical simulations and analyze the performance degradation due to PI. The PM-16QAM DSC signals are generated following the processing blocks shown in Fig. 1. A different pseudo-random binary sequence (PRBS) of degree 16 is used for each SC, with 10 repetitions, and the SC symbol rate is $R_s = 4$ Gbaud. The roll-off factor and filter length are varied throughout the simulations, and the SC spacing follows the roll-off factor such that $\Delta f = R_s(1+\rho)$, unless mentioned otherwise. A T/2-spaced 2×2 complex MIMO feed-forward equalizer used for polarization demultiplexing and equalization. The equalizer employs the least mean square (LMS) algorithm and approximates an ideal MMSE equalization. Finally, symbol decisions are performed and the bit error ratio (BER) is calculated by counting errors per SC.

Throughout the simulations, the power level of ONU#1 and ONU#3 (shown in Fig.1 inset) is kept constant while their FO is zero. In contrast, the power of SC#1 (ONU 2) is increased and its spectrum is frequency-shifted toward SC#2 (ONU#3) to emulate PI and transmitter laser FO. Consequently, SC#2 is the affected subcarrier, experiencing increased inter-subcarrier crosstalk from one neighboring SC, and all presented results correspond to this SC. Figure 4 present the OSNR penalty due to SC PI for a roll-off factor of 0.05, considering both time-domain simulations and the frequency-resolved model. The results are shown for two BER targets, namely 10^{-2} and 2×10^{-2}, as examples of pre-forward error correction (FEC) thresholds required to achieve zero uncorrected FEC frames [3]. It should be noted that, although we present the OSNR penalty, it is equivalent to the ROP penalty when using a non-optically amplified coherent receiver [13].

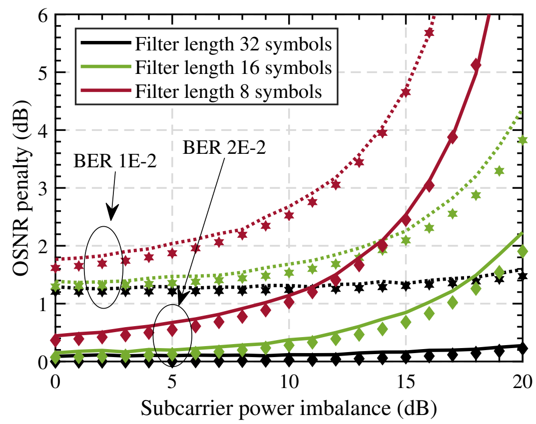

Fig. 4: Optical signal-to-noise ratio penalty versus SC power imbalance for transmitter pulse-shaping filter of different lengths (in symbols), with roll-off factors of 0.05 and 2 BER targets. Lines represent time-domain simulations, while markers correspond to the frequency-resolved model.

As observed, good agreement is achieved between the two approaches, with a discrepancy of less than 0.5 dB for an OSNR penalty of less than 6 dB. Moreover, for power imbalances below 10 dB, the model accuracy is very good, below 0.15 dB. For this roll-off factor, the OSNR penalty is negligible when a large filter length (i.e., 32 symbols) is employed regardless of the SC PI. Reducing the filter length to 16 symbols leads to a penalty that increases with the PI level, up to 2 dB for a PI of 20 dB and BER of 2×10^{-2}. The penalty further increases when a filter length of 8 symbols is used, reaching approximately 1.5 and 2.5 dB for PIs of 12 and 15 dB at BER of 2×10^{-2}, respectively.

In Fig. 5, the OSNR penalty is presented for a roll-off factor of 0.2, considering a SC spacing of either $R_s(1+\rho) = 4.8$ GHz or 4.2 GHz as in the previous setup (i.e when the roll-off factor is 0.05). For a spacing of 4.8 GHz, the OSNR penalty remains negligible with respect to PI using filter lengths of 16 symbols and above, and is around 1 dB when a filter length of 8 symbols is used with a PI of 20 dB. In contrast, decreasing the

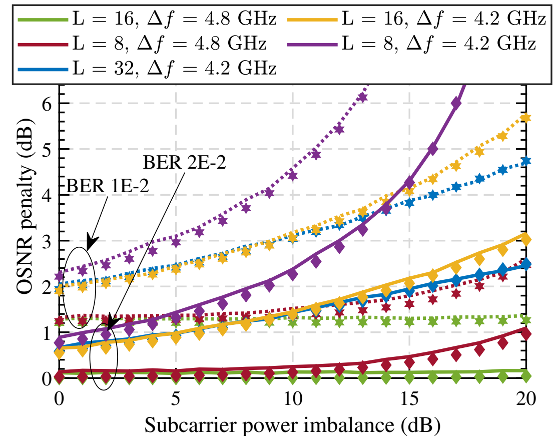

Fig. 5: Optical signal-to-noise ratio penalty versus SC PI for transmitter pulse-shaping filter of different lengths L (in symbols), with a roll-off factor of 0.2, considering two BER targets and two SC spacings Δf. Lines represent time-domain simulations, while markers correspond to the frequency-resolved model. Solid lines indicate a BER of 2×10^{-2}, and dotted lines indicate a BER of 10^{-2}.

SC frequency spacing to 4.2 GHz results in a higher penalty that exceeds 2 dB even for a filter length of 32 and BER of 2×10^{-2}. This penalty reaches up to 4 dB at a PI of 15 dB, and is higher compared to the case with $\rho = 0.05$ (2.5 dB) when using the same filter length of 8 symbols. Employing a roll-off factor of 0.2 with eight SCs requires an additional bandwidth of 4.8 GHz, which in turn necessitates higher DAC and ADC sampling rates. Otherwise, a lower roll-off factor and consequently higher spectral efficiency requires a longer impulse response and its corresponding computational cost to avoid performance degradation due to truncation errors and inter-subcarrier interference.

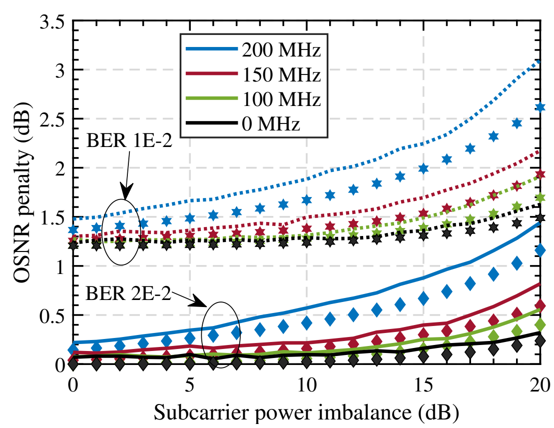

Fig. 6: Optical signal to noise ratio penalty versus SC PI corresponding to various SC TX frequency offset for two different BER targets 10^{-2} (dotted lines) and 2×10^{-2} (solid lines). Lines are for the time-domain simulations and markers are for the frequency-resolved model.

The impact of FO combined with PI is depicted in Fig. 6, considering a roll-off factor of 0.05, a filter length of 32 symbols, and both time-domain simulations and the frequency-resolved model. The FO originates from the left SC only, as described in the simulation setup, and although this offset is correctly compensated for the left SC, it still affects the neighboring SC, whose penalty increases with the PI. Both the frequency-resolved model and time-domain simulations show good agreement, with discrepancies of less than 0.5 dB, and exhibit the same trend with respect to PI. As seen, increasing the FO leads to a higher OSNR penalty, reaching approximately 1 dB and 1.5 dB for PIs of 15 dB and 20 dB, respectively, with a 200 MHz frequency shift. It is important to note that this offset penalty strongly depends on the SC frequency spacing, with smaller spacings resulting in higher penalties.

V. Conclusion

We employed a frequency-resolved model to investigate the impact of subcarrier power imbalance on the performance of future DSCM-PON systems. The goal of our work is two-fold: on one side, we presented an analytical frequency-resolved model that can obtain system performance estimation in a much smaller CPU/GPU time than time domain simulations, that were used here only to confirm the validity of the proposed analytical model. On another side, we show how the model can be effectively used to predict system penalties and thus to properly dimension the transceiver DSP free parameters, such as the filters used for the DSCM shaping and detection.

We showed in particular that power imbalance between upstream SC degrades system performance through linear inter-subcarrier crosstalk arising from physical impairments, including finite pulse-shaping filters, and laser non-idealities. This degradation can range from 1 dB to more than 6 dB (inside the parameter space that we spanned) and provides insight into how transmitter power should be pre-leveled. Using a lower roll-off factor to improve spectral efficiency requires a larger number of filter taps; otherwise, the subcarrier spacing should be increased to mitigate the power imbalance penalty. Similarly, transmitter laser frequency control is required to avoid subcarrier overlapping, and it becomes even more critical under the large dynamic power ranges in PON systems.

Future investigations should consider the joint impact of power imbalance with other impairments in DSCM transmission, in particular quantization effects in the OLT receiver ADC and nonlinear effects in the ONUs optoelectronics and in the fiber.

Acknowledgment

This work has received funding from the European Union's Horizon Europe research and innovation programme under the Marie Skłodowska-Curie grant agreement No. 101073265 (EWOC). Views and opinions expressed are however those of the authors only and do not necessarily reflect those of the European Union. The European Union cannot be held responsible for them. The Authors are with the Politecnico di Torino PhotoNext Center for Applied Photonics.

References

[1] D. Zhang, D. Liu, and D. Nesset, "Progress of very high speed PON in ITU-T [invited]," *J. Opt. Commun. Netw.*, vol. 18, pp. A112–A122, Feb 2026.

[2] R. Gaudino, "Coherent PON: Recent evolutions and expected trends," in *Optical Fiber Communication Conference (OFC) 2025*, p. M2I.1, Optica Publishing Group, 2025.

[3] Z. Jia, H. Zhang, K. Choutagunta, and L. A. Campos, "Coherent passive optical network: applications, technologies, and specification development [invited tutorial]," *J. Opt. Commun. Netw.*, vol. 17, pp. A71–A86, Jan 2025.

[4] J. Li, R. Fan, Q. He, M. Luo, and X. Li, "Bidirectional TFDM 200 G coherent PON with a simplified receiver at the ONU side," *Opt. Lett.*, vol. 49, no. 18, pp. 5127–5130, 2024.

[5] T. Duthel, C. R. Fludger, B. Liu, S. Ranzini, A. Napoli, N. Sölch, S. M. Bilal, S. B. Amado, S. Alreesh, J. Sime, A. Rashidinejad, S. Erkilinc, J. Diniz, A. Kakkar, D. F. Bendimerad, M. Chagnon, A. Mathur, V. Dominic, P. Samra, H. Ahlfeldt, M. Olson, H. Sun, A. Somani, and D. F. Welch, "DSP design for coherent optical point-to-multipoint transmission," *J. Lightwave Technol.*, vol. 42, no. 3, pp. 1109–1118, 2024.

[6] M. Xu, Z. Jia, H. Zhang, L. A. Campos, and C. Knittle, "Intelligent burst receiving control in 100G coherent PON with 4×25G TFDM upstream transmission," in *Optical Fiber Communication Conference (OFC) 2022*, p. Th3E.2, Optica Publishing Group, 2022.

[7] S. Mumtaz, T.-H. Nguyen, A. Hraghi, A. Lorences-Riesgo, Y. Frignac, G. Charlet, and Y. Zhao, "Impact of laser impairments on DSCM-based 800G point-to-multipoint coherent transmission systems," in *Optical Fiber Communication Conference (OFC) 2023*, p. Th1E.3, Optica Publishing Group, 2023.

[8] S. Ranzini, C. R. S. Fludger, T. Duthel, B. Liu, A. Napoli, A. Kumpera, A. Rashidinejad, A. Kakkar, M. Missey, V. Dominic, P. Samra, H. Sun, R. Maher, A. Somani, and D. Welch, "Local and remote laser frequency control in point-to-multipoint networks using digital subcarriers," in *49th European Conference on Optical Communications (ECOC 2023)*, vol. 2023, pp. 807–810, 2023.

[9] P. Torres-Ferrera, G. Parisi, G. Rizzelli, R. Gaudino, and A. Napoli, "Analytical model for performance estimation of coherent digital subcarrier multiplexing systems affected by filtering, optical and electrical noise," in *2024 24th International Conference on Transparent Optical Networks (ICTON)*, pp. 1–5, 2024.

[10] G. Rizzelli and R. Gaudino, "Planning tools for next-generation DSP-based passive optical networks above 50G [invited tutorial]," *J. Opt. Commun. Netw.*, vol. 16, no. 7, pp. C88–C96, 2024.

[11] G. Rizzelli and R. Gaudino, "High-speed PON solutions: recent evolutions and expected trends [invited tutorial]," *J. Opt. Commun. Netw.*, vol. 18, no. 2, pp. A134–A149, 2026.

[12] G. Rizzelli, P. Torres-Ferrera, and R. Gaudino, "An analytical model for coherent transmission performance estimation after generic jones matrices," *J. Lightwave Technol.*, vol. 41, no. 14, pp. 4582–4589, 2023.

[13] S. A. zoubi and R. Gaudino, "Modeling and analysis of coherent metro + PON converged networks for ultra-high speed applications," *J. Opt. Commun. Netw.*, vol. 17, pp. 294–308, Apr 2025.